Pergamon

Int. J. Solids Structures Vol. 35, No. 15, pp. 1763–1783, 1998

0020–7683/98 $19.00 – .00

PII: S0020–7683(97)00132–7

DOMAIN INTEGRAL FORMULATION FOR STRESS INTENSITY FACTOR COMPUTATION ALONG CURVED THREE-DIMENSIONAL INTERFACE CRACKS

M. GOSZ
Department of Mechanical, Materials, and Aerospace Engineering, Illinois Institute of Technology, Chicago, IL 60616-3793, U.S.A.

J. DOLBOW and B. MORAN
Department of Civil Engineering, Northwestern University, Evanston, IL 60208, U.S.A.

(*Received* 23 *November* 1996; *in revised form* 13 *May* 1997)

Abstract—New domain integrals for extracting mixed-mode stress intensity factors along curved, three-dimensional bimaterial interface cracks are derived. In the derivation, the asymptotic auxiliary fields for the plane problem of a bimaterial interface crack are imposed along a curved crack front. The general crack-tip interaction integral (a contour integral surrounding a point on the crack front which is evaluated in the limit as the contour is shrunk onto the crack tip) is then expressed in domain form which is more suitable for numerical computation. A consequence of imposing the auxiliary fields along a curved crack front is that the auxiliary stress fields do not satisfy equilibrium, and the auxiliary strain fields do not satisfy compatibility. The terms which arise due to the lack of equilibrium and compatibility are not sufficiently singular to contribute to the crack-tip interaction integral or to affect its path independence; however, these terms become important when domain integral representations are introduced, because they involve fields which are not asymptotically close to the crack tip. In order to compute the pointwise stress intensity factors along the crack front, the domain integrals are evaluated as a post-processing step in the finite element method. In the numerical results, it is demonstrated that it is crucial to incorporate the terms that arise due to lack of equilibrium and compatibility of the auxiliary fields, especially in regions where the local crack front curvature is high. In the paper, we present two numerical examples. As a benchmark, we first consider the problem of a penny-shaped interface crack embedded in a cylinder. The results for the complex stress intensity factor and phase angle are found to be in excellent agreement with the analytical solution. The problem of an elliptical crack embedded between two dissimilar isotropic materials is also considered, and the results are discussed. © 1998 Elsevier Science Ltd.

1. INTRODUCTION

The overall mechanical properties of advanced composite materials depend heavily on the nature of the bond at bimaterial interfaces. Unfortunately, interfacial delamination and fracture are commonly observed problems that may ultimately limit the use of these materials (ranging from ceramic and metal matrix composites for the aerospace industry to nanoscale structures for the microelectronics industry). The need to improve fracture toughness has led to significant progress recently in the area of interfacial fracture mechanics. Excellent review articles on the subject have been written by Rice *et al.* (1988), Shih (1990), and Hutchinson and Suo (1991).

Among the available methods for calculating fracture parameters, the domain integral method has emerged as being well suited for bimaterial interface crack problems. In the domain integral method, a crack-tip contour integral is expressed as a volume integral over a finite domain surrounding the crack tip. The process of recasting the contour integral into a volume integral is advantageous for numerical purposes, because accurate fracture parameters can be obtained without having to precisely capture the details of the singular fields in the vicinity of the crack tip, see Moran and Shih (1987a,b) for a general discussion on crack-tip contour integrals and their associated domain integral representation. The domain integral method has been employed by Li *et al.* (1985) and by Shih *et al.* (1986) to determine the energy release rate along straight, three-dimensional crack fronts in

homogeneous solids. Shih and Asaro (1988) have employed domain forms of interaction energy integrals to extract mixed-mode stress intensity factors in planar bimaterial crack problems. Nakamura and Parks (1989), and Nakamura (1991) have used this same approach to determine the mixed-mode stress intensity factors along straight, three-dimensional bimaterial interface cracks. Nikishkov and Atluri (1987) have developed a domain integral approach to determine mixed-mode stress intensity factors along planar three-dimensional crack fronts in homogeneous solids.

Domain representations of interaction energy integrals to extract mixed-mode stress intensity factors for axisymmetric bimaterial crack problems have been derived recently by Nahta and Moran (1993). In their work, they recognized that when the auxiliary fields that appear in the integrand of the interaction integrals are imposed along a curvilinear crack front, the auxiliary stress fields do not satisfy equilibrium, and the auxiliary strain fields violate compatibility. Because of the lack of equilibrium and compatibility, along with other local curvature effects, they appropriately incorporated additional terms (that ordinarily vanish for straight bimaterial interface cracks) in the resulting domain integrals.

In the present paper, we extend the work of Nahta and Moran (1993) to the general three-dimensional case. In particular, we derive new domain integrals for extracting mixed-mode stress intensity factors along curved bimaterial interface cracks, and we describe a straightforward approach, which involves a post-processing step in the finite element method, for evaluating the resulting domain integrals. Also, in the numerical results section of the paper, we illustrate the importance of incorporating additional terms in the domain integrals which arise due to crack front curvature.

To outline the paper, in the following section we describe the interaction energy integral approach for extracting mixed-mode stress intensity factors along curved, three-dimensional crack fronts. In Section 3, we derive the domain representation of the interaction energy integrals and discuss some of the key difficulties encountered in the evaluation of the resulting domain integrals. In Section 4, we present the numerical results for two example problems. First we consider the case of a penny-shaped crack embedded between two dissimilar isotropic materials subjected to remote tension and compare the present numerical results with the analytical solution. Second, to demonstrate our present capabilities for the case of a general curvilinear bimaterial interface crack, we consider the problem of an elliptical crack embedded between two different isotropic materials and the results are discussed. Finally, in Section 5 we give a brief summary and some concluding remarks.

2. EXTRACTION OF MIXED-MODE STRESS INTENSITY FACTORS ALONG CURVED BIMATERIAL INTERFACE CRACKS

In this section, we present the methodology for calculating the mixed-mode stress intensity factors along three-dimensional, curved bimaterial interface cracks. We begin by considering the curvilinear crack front as shown in Fig. 1. As shown in the figure, we define a local orthogonal coordinate system at a point s along the crack front such that the local x_2 axis is perpendicular to the plane of the crack, and the x_1 and x_3 axes lie in the plane of the crack and are normal and tangent respectively to the crack front. Following Nahta and

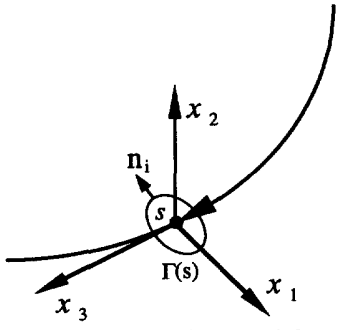

Fig. 1. General curvilinear crack front.

Moran (1993), the general crack-tip contour integral along the three-dimensional crack front takes the form

$$I(s) = \lim_{\Gamma \to 0} \xi_l(s) \int_{\Gamma(s)} P_{lj} n_j \, d\Gamma \tag{1}$$

where $\Gamma(s)$ is a contour in the local $x_1 - x_2$ plane surrounding point s on the crack front, $\xi_l(s)$ is the local crack extension, and n_j is the unit outward normal to the contour Γ (see Fig. 1). When the tensor P_{lj} in eqn (1) is replaced by the energy momentum tensor (Eshelby, 1956, 1970), i.e.,

$$P_{lj} = W\delta_{lj} - \sigma_{ij} u_{i,l} \tag{2}$$

and the vector $\xi_l(s)$ is defined as the unit outward normal to the crack front in the local $x_1 - x_3$ plane, the crack-tip integral (1) yields the energy release rate $G(s)$ due to crack extension in its own plane. Here in eqn (2), W is the strain energy density, σ_{ij} are the components of the Cauchy stress, u_i are the displacement components, and the comma denotes partial differentiation with respect to the spatial coordinates.

A particularly convenient method for extracting mixed-mode stress intensity factors is the interaction energy integral approach. Shih and Asaro (1988) have employed interaction energy integrals to evaluate mixed-mode stress intensity factors in two-dimensional plane problems. Nakamura and Parks (1989), and Nakamura (1991), have used this approach for obtaining mixed-mode stress intensity factors along three-dimensional *straight* crack fronts. It is emphasized that in the present paper, the interaction energy integrals are developed for extracting mixed-mode stress intensity factors along *curved* three-dimensional cracks. Because the present three-dimensional interaction energy integral approach is based upon the assumption that the near-tip crack fields asymptote to the plane and antiplane strain fields, the present development is not strictly applicable to crack fronts near a free surface where the state of plane stress dominates. The latter case has been investigated by Nakamura (1991) for the case of straight bimaterial interface cracks intersecting a free surface. It turns out that at the intersection of the crack and the free surface, the singularity is more severe than the usual $1/\sqrt{r}$ singularity. However, this singularity dominates only in a very small region near the free surface. Plane strain conditions prevail outside this small region, see Nakamura (1991) for more detail.

The interaction energy integral $I(s)$ can be obtained by substituting the following expression for the tensor P_{lj} in the general crack-tip integral (1):

$$P_{lj} = \sigma_{ik} - u^{aux}_{i,l} \sigma_{ij} - u_{i,l}. \tag{3}$$

Hence,

$$I(s) = \lim_{\Gamma \to 0} \xi_l(s) \int_{\Gamma(s)} (\sigma^{aux}_{ik} \varepsilon^{aux}_{ik} \delta_{lj} - u^{aux}_{i,l} \sigma_{ij} - u_{i,l} \sigma^{aux}_{ij}) n_j \, d\Gamma \tag{4}$$

where u^{aux}_i, ε^{aux}_{ij}, and σ^{aux}_{ij} are the auxiliary displacement, strain and stress fields which will be defined in the following section.

2.1. *Interfacial fracture mechanics*

Before defining the auxiliary fields that appear in the interaction energy integral (4), we first provide a brief summary of the pertinent quantities that arise when dealing with cracks in bimaterials. Consider the plane problem of an interface crack between two

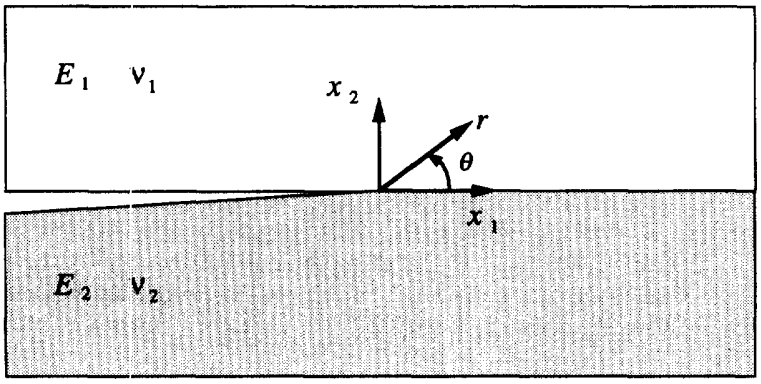

Fig. 2. Plane problem of an interface crack between two dissimilar isotropic materials.

dissimilar isotropic materials as shown in Fig. 2. For convenience, we adopt a local polar coordinate system centered at the crack tip, and we label the material occupying the upper half-plane as material 1 with Young's modulus E_1 and Poisson's ratio ν_1. The material occupying the lower half-plane has moduli E_2 and ν_2.

Using the notation of Rice *et al.* (1990), the near-tip stress fields can be written as

$$\sigma_{ij} = \frac{1}{\sqrt{2\pi r}}\{\mathrm{Re}[\mathbf{K}r^{i\varepsilon}]\tilde{\sigma}_{ij}^{I}(\theta,\varepsilon) + \mathrm{Im}\,[\mathbf{K}r^{i\varepsilon}]\tilde{\sigma}_{ij}^{II}(\theta,\varepsilon) + K_{III}\tilde{\sigma}_{ij}^{III}(\theta)\} \tag{5}$$

where $\mathbf{K} = K_I + iK_{II}$ is the complex stress intensity factor and $\tilde{\sigma}_{ij}$ are the universal angular functions which depend on the bimaterial constant ε.

Introducing the Kolosov constants

$$\kappa_i = \begin{cases} 3-4\nu_i & \text{plane strain} \\ \dfrac{3-\nu_i}{1+\nu_i} & \text{plane stress} \end{cases} \tag{6}$$

along with Dundurs' constants

$$\alpha = \frac{\mu_1(\kappa_2+1)-\mu_2(\kappa_1+1)}{\mu_1(\kappa_2+1)+\mu_2(\kappa_1+1)}$$
$$\beta = \frac{\mu_1(\kappa_2-1)-\mu_2(\kappa_1-1)}{\mu_1(\kappa_2+1)+\mu_2(\kappa_1+1)} \tag{7}$$

the bimaterial constant ε can be defined as

$$\varepsilon = \frac{1}{2\pi}\ln\left(\frac{1-\beta}{1+\beta}\right). \tag{8}$$

The in-plane traction vector $\mathbf{t}$ transmitted across the interface at a distance r ahead of the crack tip can be related to the complex stress intensity factor $\mathbf{K}$ through

$$\mathbf{t} = [\sigma_{22}(r,0) + i\sigma_{12}(r,0)] = \frac{\mathbf{K}r^{i\varepsilon}}{\sqrt{2\pi r}}. \tag{9}$$

We note that the complex stress intensity factor has the dimensions $[stress][length]^{1/2-i\varepsilon}$. The phase angle ψ is defined as the ratio of shear to normal in-plane tractions transmitted across the interface at a distance r ahead of the crack tip. Thus, ψ is given by

$$\psi = \frac{\sigma_{12}(r,0)}{\sigma_{22}(r,0)} = \frac{\mathrm{Im}[\mathbf{K}r^{i\varepsilon}]}{\mathrm{Re}[\mathbf{K}r^{i\varepsilon}]}. \tag{10}$$

The phase angle ψ plays an important role in the initiation and direction of interface crack growth and hence is an important parameter in the characterization of interfacial fracture toughness. We note that in reporting the phase angle ψ for a particular loading configuration and geometry, a length quantity L must be specified. While the choice of L is arbitrary, in practice it is typically chosen to be a characteristic length such as crack length or specimen size.

The energy release rate G can be expressed in terms of the stress intensity factors through the relation

$$G = \frac{1}{E^*}\frac{\mathbf{K}\bar{\mathbf{K}}}{\cosh^2(\pi\varepsilon)} + \frac{K_{III}^2}{2\mu^*} \tag{11}$$

were

$$E^* = \frac{2E_1'E_2'}{E_1'+E_2'}$$

$$\mu^* = \frac{2\mu_1\mu_2}{\mu_1+\mu_2} \tag{12}$$

and

$$E' = \begin{cases} \dfrac{E}{1-\nu^2} & \text{plane strain} \\ E & \text{plane stress} \end{cases}. \tag{13}$$

2.2. *Auxiliary fields*

As a point s lying on a curved three-dimensional crack front is approached in the local x_1-x_2 plane, the near-tip fields asymptotically approach the plane and antiplane crack-tip fields described in the previous section. Therefore, if the auxiliary fields that appear in the integrand of the interaction energy integral (4) are defined to be the plane and antiplane fields in the local x_1-x_2 plane with local stress intensity factors K_I^{aux}, K_{II}^{aux}, and K_{III}^{aux}, the interaction energy integral is locally path-independent and, in the limit as $\Gamma \to 0$, takes the value

$$I(s) = \frac{2}{E^*\cosh^2(\pi\varepsilon)}[K_IK_I^{aux} + K_{II}K_{II}^{aux}] + \frac{1}{\mu^*}K_{III}K_{III}^{aux}. \tag{14}$$

Thus, the process of evaluating the mixed-mode stress intensity factors involves making a judicious choice of the auxiliary stress intensity factors, and then evaluating the interaction energy integral (4). For example, to extract K_I, we set $K_I^{aux} = 1$, $K_{II}^{aux} = K_{III}^{aux} = 0$, from which it follows from eqn (14) that

$$K_I(s) = \frac{E^*\cosh^2(\pi\varepsilon)}{2}I(s). \tag{15}$$

In order to numerically evaluate the interaction energy integrals developed in this section for the extraction of mixed-mode stress intensity factors along curved bimaterial interface cracks, it is advantageous to recast the contour integrals in their equivalent domain forms which are developed in the following section. As pointed out by Nahta and Moran (1993), a consequence of imposing the plane strain auxiliary fields along a curved crack front is that the auxiliary stress fields do not satisfy equilibrium, and the auxiliary strain fields do not satisfy the strain displacement relations (compatibility). While the terms

which give rise to lack of equilibrium and compatibility are not sufficiently singular in the asymptotic limit to contribute to the value of the interaction integrals or affect their path independence, it is important not to neglect them in the evaluation of the equivalent domain integrals (as illustrated in the numerical results section of this paper). This is because these integrals involve fields which are not asymptotically close to the crack tip.

3. DOMAIN INTEGRAL FORMULATION

In this section, we derive the equivalent domain representations of the general crack-tip contour integrals introduced in the previous section. To begin, we consider a small segment L_c of a curved crack front which lies in the local x_1-x_3 plane as shown in Fig. 3. Next, we assume that the segment undergoes a virtual crack advance in the plane of the crack, and we define the magnitude of the advance at each point s as $\Delta a(s)$. We note that $\Delta a(s)$ varies continuously along L_c and vanishes at each end of the segment. Now let

$$\bar{I} = \int_{L_c} I(s)\Delta a(s)\,\mathrm{d}s \tag{16}$$

where $I(s)$ is the general crack-tip integral defined by eqn (1). When $I(s)$ pertains to the pointwise energy release rate, $\bar{I}$ gives the total energy released when the finite segment L_c undergoes the virtual crack advance. Similarly, when $I(s)$ pertains to the interaction energy integral, $\bar{I}$ yields the total interaction energy for the virtual crack advance.

The appropriate domain forms of the pointwise interaction energy integrals and energy release rate can be obtained from eqn (16) by considering a tubular domain V surrounding the crack segment as shown in Fig. 4. As shown in the figure, the surface S_t is formed by

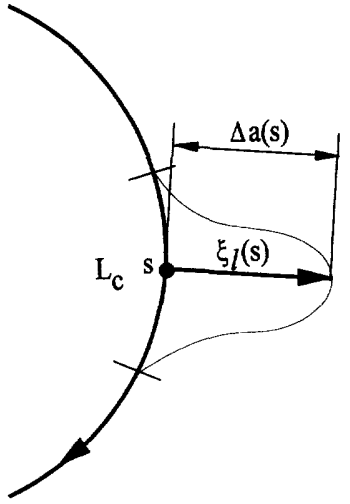

Fig. 3. Small segment of a curved crack front that undergoes a virtual crack advance $\Delta a(s)$.

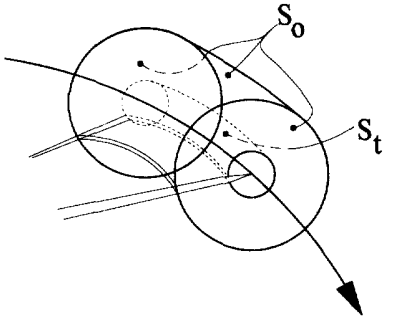

Fig. 4. Tubular domain surrounding a segment of the crack front.

translating the contour Γ along the crack segment L_c. We denote by S_o the outer surfaces of V including the ends. Next, we introduce a test function q_l which is sufficiently smooth in V and is defined on the surfaces of V as follows:

$$q_l = \begin{cases} \Delta a(s)\xi_l(s) & \text{on } S_t \\ 0 & \text{on } S_o \end{cases}. \tag{17}$$

Finally, in the limit as the tubular surface S_t is shrunk onto the crack segment L_c, in the absence of crack face tractions, we obtain the domain integral

$$I = -\int_V [\mathrm{tr}(\mathbf{P}\cdot\vec{\nabla}\mathbf{q}) + (\vec{\nabla}\cdot\mathbf{P}^{\mathrm{T}})\cdot\mathbf{q}]\,\mathrm{d}V. \tag{18}$$

A simple relationship between the domain/volume integral I and the pointwise crack-tip integral $I(s)$ can be obtained if it is assumed that $I(s)$ is constant along the small crack segment L_c. It then follows directly from (16) that

$$I(s) = \frac{I}{\displaystyle\int_{L_c} \Delta a(s)\,\mathrm{d}s}. \tag{19}$$

In practice, the evaluation of the integral that appears in the denominator of eqn (19) is straightforward (see Appendix A).

3.1. *Evaluation of the domain representation of the interaction integral*

In the evaluation of the energy release rate, under conditions that render the tensor $\mathbf{P}^{\mathrm{T}}$ divergence free (i.e., in the absence of body forces, thermal strains, inertia, etc.) the integral I given by eqn (18) reduces to the domain representation of the familiar J-integral, i.e.,

$$I = J = \int_{L_c} G(s)\Delta a(s)\,\mathrm{d}s = -\int_V \mathrm{tr}[(W\mathbf{I} - \vec{\nabla}\mathbf{u}\cdot\boldsymbol{\sigma})\cdot\vec{\nabla}\mathbf{q}]\,\mathrm{d}V. \tag{20}$$

The numerical evaluation of the domain integral (20) can be carried out as a straightforward post-processing step in the finite element method, see, for example, Shih *et al.* (1986) for details. Special care must be taken, however, in the evaluation of the equivalent domain form of the interaction energy integral. As discussed in Section 2, when the auxiliary fields are imposed along a curved crack front, the auxiliary stress fields do not satisfy equilibrium, and the auxiliary strain fields are not the symmetric gradient of the auxiliary displacement fields, i.e., $\boldsymbol{\varepsilon}^{aux} \neq \nabla_s \mathbf{u}^{aux}$. For these reasons, the tensor $\mathbf{P}^{\mathrm{T}}$, as defined by eqn (3), is not divergence free, and the equivalent domain form of the interaction integral is given by eqn (18) with

$$(\vec{\nabla}\cdot\mathbf{P}^{\mathrm{T}}) = \boldsymbol{\sigma}:(\boldsymbol{\varepsilon}^{aux}\vec{\nabla} - \vec{\nabla}\mathbf{u}^{aux}\vec{\nabla}) - (\vec{\nabla}\mathbf{u})\cdot(\vec{\nabla}\cdot\boldsymbol{\sigma}^{aux}) \neq 0. \tag{21}$$

Equation (21) can be expressed in Cartesian components as

$$\sigma_{ij}\varepsilon^{aux}_{ij,k} - \sigma_{ij}u^{aux}_{j,ik} - \sigma^{aux}_{ij,i}u_{j,k} \neq 0. \tag{22}$$

The main difficulty in calculating the interaction energy integral lies in the evaluation of the gradients and higher order gradients of the auxiliary fields that appear in the integrand. To illustrate a convenience procedure to evaluate these gradients, we consider a point p

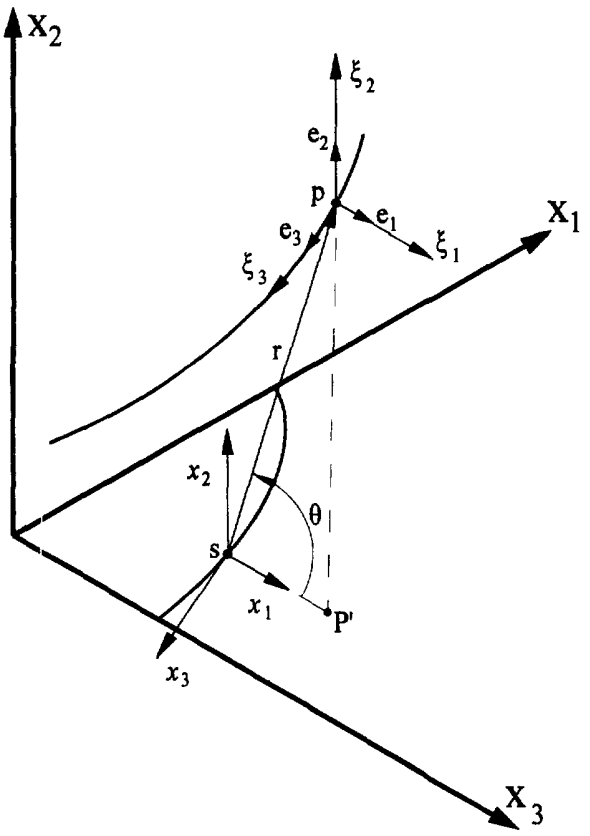

Fig. 5. Local curvilinear coordinate system.

which lies in the local x_1-x_2 plane as shown in Fig. 5. Next, we construct an orthogonal ξ_1, ξ_2, ξ_3 curvilinear coordinate system with base vectors $\mathbf{e}_1$, $\mathbf{e}_2$, and $\mathbf{e}_3$ as shown in the figure. We note that the ξ_1 and ξ_2 axes form straight lines which are parallel to the x_1 and x_2 axes, respectively, and the coordinate curve ξ_3 is formed by keeping the polar coordinates r and θ shown in the figure fixed and moving along the crack front s. Because the auxiliary fields do not vary along the coordinate curve ξ_3, it is convenient to express the components of the gradients of the auxiliary fields at point p in the curvilinear coordinate system. For example, in the extraction of the mode I and mode II stress intensity factors, u_1^{aux} and u_2^{aux} are the only nonzero auxiliary displacement components. For this case, the gradient of the auxiliary displacement field at point p is written as

$$\vec{\nabla}\mathbf{u}^{aux} = \left(\mathbf{e}_1 \frac{\partial}{\partial \xi_1} + \mathbf{e}_2 \frac{\partial}{\partial \xi_2} + \mathbf{e}_3 \frac{\partial}{\partial \xi_3}\right) \otimes (u_1^{aux}\mathbf{e}_1 + u_2^{aux}\mathbf{e}_2) \tag{23}$$

and the components are given by

$$[\vec{\nabla}\mathbf{u}^{aux}] = \begin{bmatrix} u_{1,1}^{aux} & u_{2,1}^{aux} & 0 \\ u_{1,2}^{aux} & u_{2,2}^{aux} & 0 \\ 0 & 0 & u_1^{aux}/\rho \end{bmatrix}. \tag{24}$$

In eqn (24), ρ is the local radius of curvature of the coordinate curve ξ_3 evaluated at point p. We note that the local radius of curvature ρ is related to the local radius of curvature ρ_s of the crack front at point s through the relation

$$\rho = \rho_s + x_1^p \tag{25}$$

where x_1^p is the local x_1 coordinate of point p.

In the calculation of the mode III stress intensity factor, u_3^{aux} is the only nonzero auxiliary displacement component, and thus for this case we have,

$$\vec{\nabla} u^{aux} = \left(\mathbf{e}_1 \frac{\partial}{\partial \xi_2} + \mathbf{e}_2 \frac{\partial}{\partial \xi_2} + \mathbf{e}_3 \frac{\partial}{\partial \xi_3} \right) \otimes (u_3^{aux} \mathbf{e}_3) \tag{26}$$

$$[\vec{\nabla} \mathbf{u}^{aux}] = \begin{bmatrix} 0 & 0 & u_{3,1}^{aux} \\ 0 & 0 & u_{3,2}^{aux} \\ -u_3^{aux}/\rho & 0 & 0 \end{bmatrix}. \tag{27}$$

For the sake of completeness, the details of the finite element evaluation of the domain representations for the energy release rate and the interaction energy integrals are given in Appendix A. In addition, we have provided the explicit forms (in terms of the polar coordinates r and θ) of the auxiliary displacement fields in Appendix B. The derivatives and higher order derivatives of the auxiliary fields given in Appendix B are obtained through a repeated use of the chain rule.

4. NUMERICAL RESULTS

In order to demonstrate the accuracy and utility of the interaction energy integral formulation presented in the previous sections, we consider two numerical examples. First, we consider the case of a penny-shaped interface crack in an infinite body subjected to remote tension. Second, to illustrate the generality of the present method and the importance of retaining the curvature terms that appear in the domain integral formulation discussed in the previous section, we also consider the case of an elliptical interface crack embedded in an infinite solid subjected to remote tension.

4.1. *Penny-shaped interface crack*

As a benchmark, we consider the problem of a penny-shaped crack of radius a embedded in an infinite solid subjected to the remote tension σ_o. The analytical solution for the complex stress intensity factor $\mathbf{K}$ has been obtained by Kassir and Bregman (1972) and is given as

$$K_I + iK_{II} = 2\sigma_o \sqrt{a} \frac{\Gamma(2+i\varepsilon)}{\Gamma(\frac{1}{2}+i\varepsilon)} (2a)^{-i\varepsilon} \tag{28}$$

where Γ is the gamma function, and ε is the bimaterial constant.

The details of the three-dimensional model employed in the numerical calculation are shown in Fig. 6. As shown in the figure, we consider the material combination of glass ($E_1 = 1 \times 10^7$ psi, $\nu_1 = 0.22$) bonded to steel ($E_2 = 3 \times 10^7$ psi, $\nu_2 = 0.3$) which yields a bimaterial constant $\varepsilon = 0.06557$ with $E^* = 1.594 \times 10^7$ psi. Denoting the radius of the crack, the outer radius of the cylinder, and the height of the cylinder by the parameters a, b, and h respectively, the geometry of the model was chosen such that $a/b = 0.1$, and $h/b = 1.0$. These ratios were chosen so as to make any contributions to the domain integrals due to boundary effects negligible. In order to simulate the case of a penny-shaped crack embedded in a cylinder, the following boundary conditions were enforced:

$$\begin{aligned} &x_1 = 0; \quad u_1 = 0 \\ &x_3 = 0; \quad u_3 = 0 \\ &x_2 = \pm h; \quad \sigma_{22} = \sigma_o. \end{aligned} \tag{29}$$

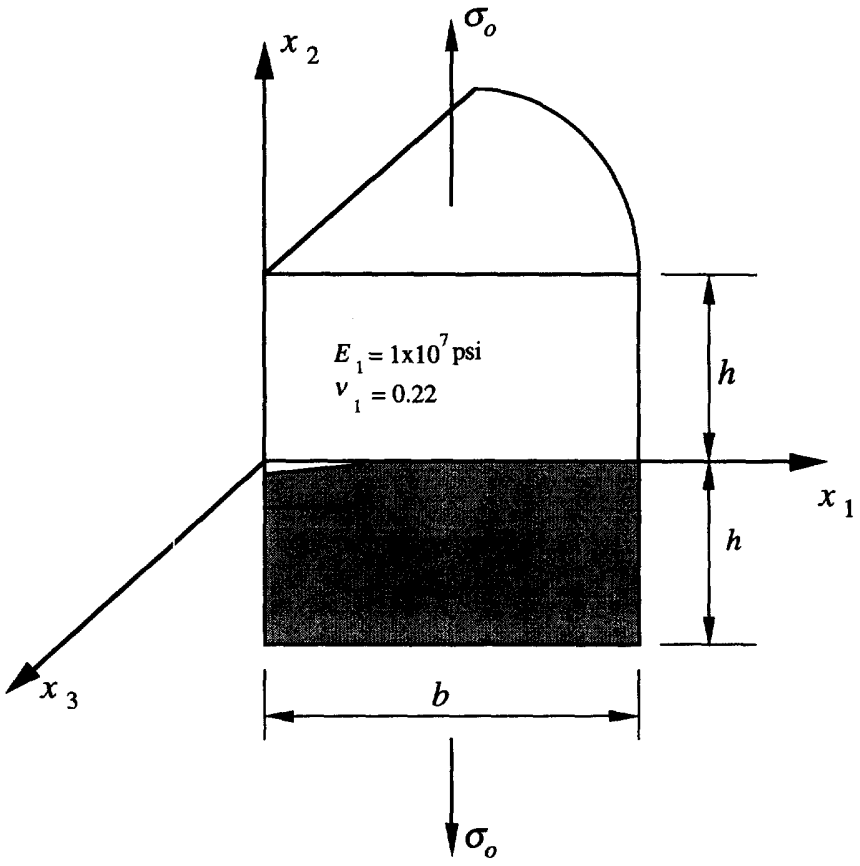

Fig. 6. Penny-shaped crack between two dissimilar isotropic materials.

The finite element mesh used in the numerical calculation is composed of 6264 eight-node brick elements (7257 nodes) and is shown in Fig. 7a. The details of the mesh in the vicinity of the crack front are shown in Fig. 7b. The finite element domains used to evaluate the domain representation of the J-integral (20) and the interaction integral (18) were constructed by sweeping a square, two-dimensional crack-tip mesh with sides of length $0.2a$ along the circular crack front while keeping the two-dimensional crack-tip mesh normal to the crack front. The smallest elements at the crack tip have a characteristic length of $0.002a$, and we emphasize that no singular elements were employed in the numerical calculations.

Normalized numerical and analytical results are shown in Table 1, where excellent agreement between the numerical and analytical results can be seen. We note that the numerical values for the stress intensity factors K_I and K_{II} reported in the table were obtained by evaluating the appropriate interaction energy integrals (18), and the energy release rate G was computed by evaluating the domain integral (20).

4.2. *Elliptical interface crack*

To demonstrate our present capabilities for the case of general curvilinear crack fronts, we consider the problem of an elliptical crack embedded between two dissimilar isotropic

Table 1. Comparison of the numerical results with the analytical solution for a penny-shaped interface crack under remote tension.

	$\frac{\pi E^* \cosh^2(\pi\varepsilon) G}{4\sigma_o^2 a}$	$\frac{\sqrt{\pi}\,\mathrm{Re}\,[\mathbf{K}(2a)^{i\varepsilon}]}{2\sigma_o\sqrt{(a)}}$	$\frac{\sqrt{\pi}\,\mathrm{Im}\,[\mathbf{K}(2a)^{i\varepsilon}]}{2\sigma_o\sqrt{(a)}}$	ψ	$\frac{GE^* \cosh^2(\pi\varepsilon)}{\mathbf{K}\bar{\mathbf{K}}}$
Analytical	1.0185	0.9969	0.1565	0.1557	1.000
Numerical	0.9509	0.9659	0.1524	0.1564	0.994
% error	−6.6%	−3.1%	−2.63%	0.48%	−0.56%

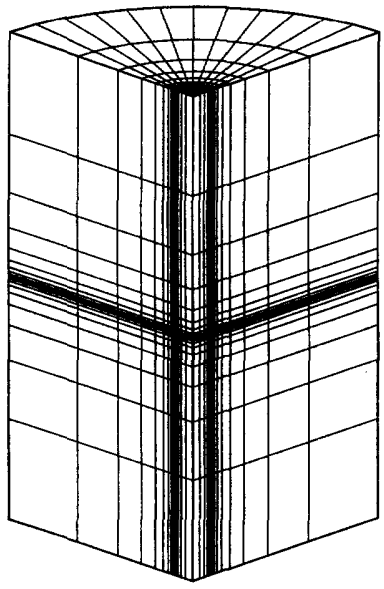

(a)

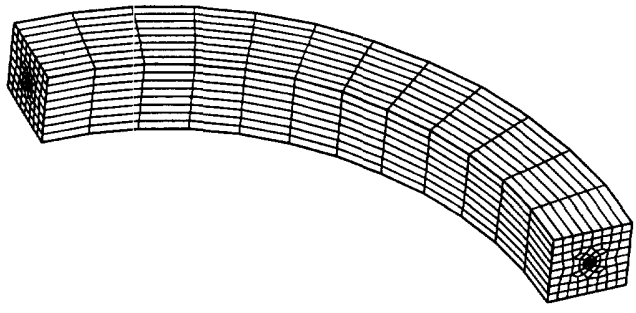

(b)

Fig. 7. The finite element mesh used for the penny-shaped crack problem (a), and details of the mesh in the vicinity of the crack front (b). The mesh is composed of 6264 eight-node brick elements (7257 nodes).

materials subjected to the remote tension σ_o. Utilizing symmetry, it is only necessary to consider one-quarter of the problem as shown in Fig. 8. As shown in the figure, the elliptical crack front is characterized by the aspect ratio a/c, and the characteristic dimensions W and h are chosen so that the boundary correction factors for this particular geometry can be considered negligible. In the present analysis, we have chosen the dimensionless ratios as follows:

$$\begin{aligned} a/c &= 0.4 \\ W/c &= 10.0 \\ h/W &= 1.0. \end{aligned} \tag{30}$$

The boundary conditions applied to the quarter model are given by (29), and the finite element mesh is composed of 6340 eight-node brick elements (7548 nodes) as shown in Fig. 9a. Again, the details of the mesh in the vicinity of the crack front are generated by sweeping

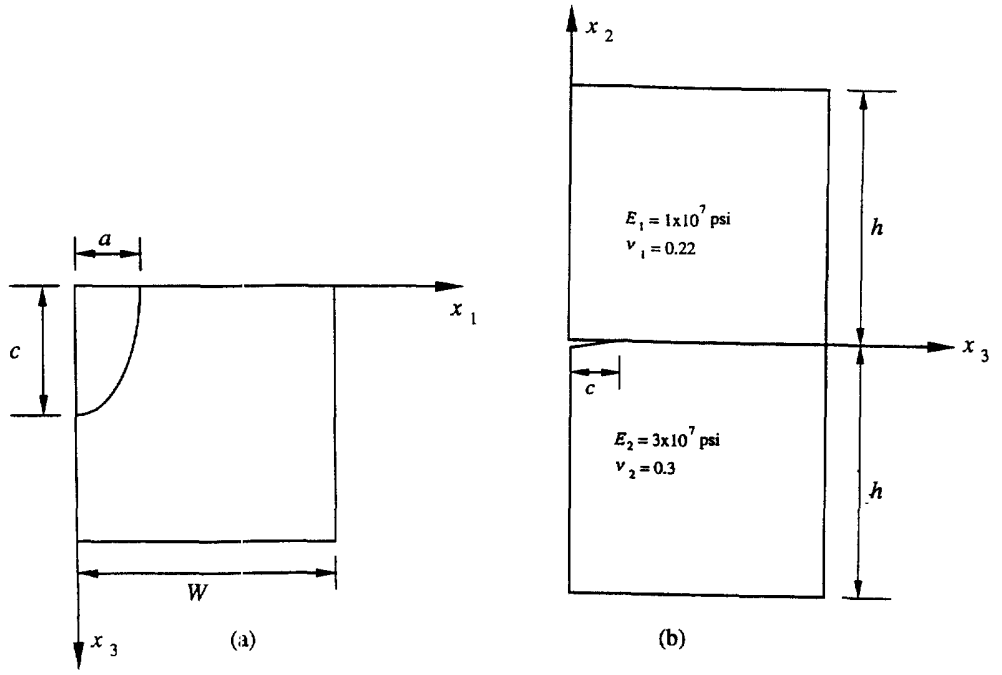

Fig. 8. Elliptical crack embedded between two dissimilar isotropic materials. Top view (a), and side view (b).

a two-dimensional crack-tip mesh along the elliptical crack front as shown in Fig. 9b. Here, the two-dimensional crack-tip mesh has sides of length $0.2c$, and the characteristic length of the smallest elements near the crack tip is $0.002c$.

The analytical solution for the mode I stress intensity factor for the case of an elliptical crack embedded in an infinite homogeneous and isotropic solid has been obtained by Irwin (1962). His result can be written as

$$K_I = \sigma_o \sqrt{\frac{\pi a}{Q}} \left\{ \sin^2 \phi + \frac{a^2}{c^2} \cos^2 \phi \right\}^{1/4} \tag{31}$$

where the quantity Q is the square of an elliptical integral of the second kind given by

$$Q = \left\{ \int_0^{\pi/2} \left[1 - \frac{c^2 - a^2}{c^2} \sin^2 \phi \right]^{1/2} d\phi \right\}^2 \tag{32}$$

and ϕ is the parametric angle which is defined in Fig. 10.

The numerical results for the homogeneous case are compared with the analytical solution as shown in Fig. 11 where the normalized mode I stress intensity factor is plotted versus the parametric angle ϕ. We note that the pointwise values $K_I(\phi)$ are obtained by evaluating the domain representation of the interaction integral (18). As shown in the figure, excellent agreement is obtained between the numerical and analytical results (the maximum error is less than 2%). The numerical result obtained by neglecting the terms in the integrand of the interaction integral that arise due to the local curvature of the crack front is also plotted in Fig. 11. The error between this result and the analytical solution is greater than 10% in the region where the local crack front curvature is high and decreases to about 2% in the region of low crack front curvature.

For the homogeneous case, the mode I stress intensity factor K_I is related to the energy release rate G through the relation

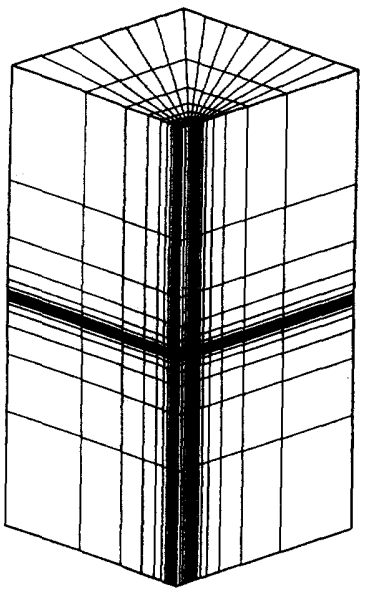

(a)

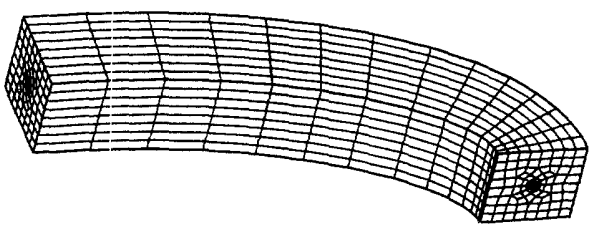

(b)

Fig. 9. The finite element mesh used for the elliptical crack problem (a), and details of the mesh in the vicinity of the crack front (b). The mesh is composed of 6340 eight-node brick elements (7548 nodes).

$$K_I^2 = E^* G. \tag{33}$$

As an additional check on the present numerical results, we also compute the pointwise energy release rate by evaluating the domain representation of the J-integral (20) and plot the ratio E^*G/K_I^2 versus ϕ as shown in Fig. 12. As shown in the figure, excellent consistency between the pointwise values of G and K_I are obtained. Here, when the curvature terms in the integrand of the interaction integral are neglected, significant error (about 18%) occurs in the region where the local crack front curvature is high.

Next, we analyze an elliptical crack embedded between two dissimilar isotropic materials. As in the penny-shaped crack example, we consider the case of glass ($E_1 = 1 \times 10^7$ psi, $\nu_1 = 0.22$) bonded to steel ($E_2 = 3 \times 10^7$ psi, $\nu_2 = 0.30$) for which $\varepsilon = 0.06557$ and $E^* = 1.594 \times 10^7$ psi. The numerical results for the normalized mode I and mode II stress intensity factors plotted versus the parametric angle ϕ are shown in Fig. 13 and Fig. 14, respectively. As shown in Fig. 14, the material mismatch causes significant mode II loading near the crack tip, and when the curvature terms are neglected, significant error is present

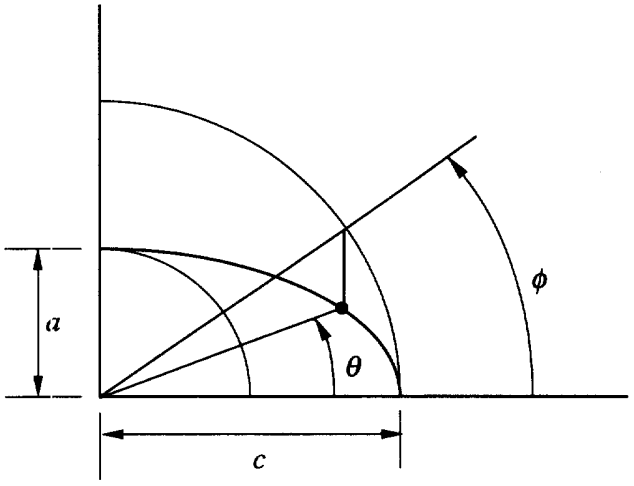

Fig. 10. Definition of the parametric angle ϕ.

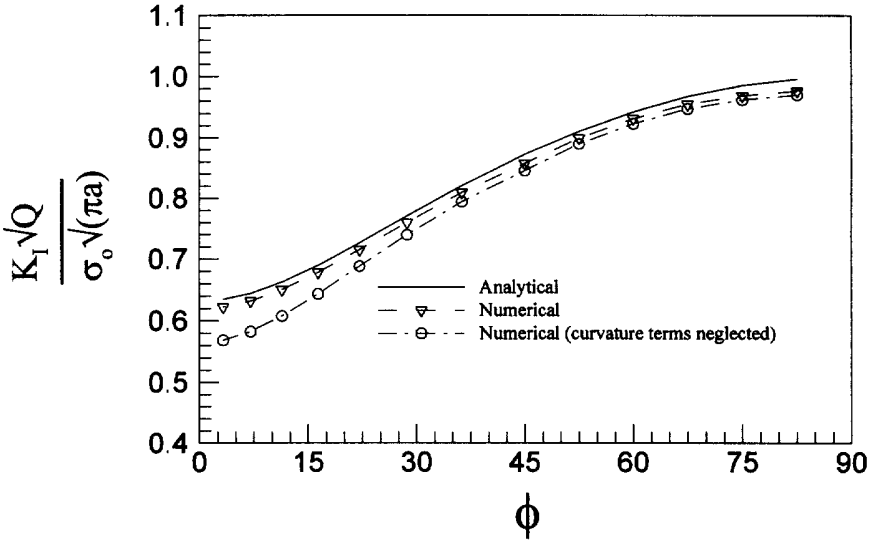

Fig. 11. Normalized mode I stress intensity factor K_I plotted vs parametric angle ϕ for the case of an elliptical crack embedded in a homogeneous solid.

in the region of high local crack front curvature, especially for the mode II stress intensity factor where the maximum error exceeds 35%. The phase angle ψ, using a characteristic length $L = 2c$, is plotted versus ϕ as shown in Fig. 15. As shown in the figure, the phase angle is relatively constant along the crack front and reaches a maximum value of approximately $\psi = 12°$ at $\phi = 21°$. Again, the phase angle is in significant error when the curvature terms are neglected.

The results for the mode III stress intensity factor along the crack front are shown in Fig. 16. To indicate the relative strength of antiplane deformation, we have defined a second phase angle φ in terms of K_{III} as follows:

$$\varphi = \cos^{-1}\left\{\frac{K_{III}}{2\mu^* G}\right\}. \tag{34}$$

Here, G is the energy release rate which is expressed in terms of the stress intensity factors in eqn (11). The phase angle φ is plotted versus parametric angle ϕ as shown in Fig. 16. As shown in the figure, the numerical results indicate that the mode III stress intensity factor is very small along the entire crack front (note that a phase angle $\varphi = 90°$ indicates $K_{III} = 0$).

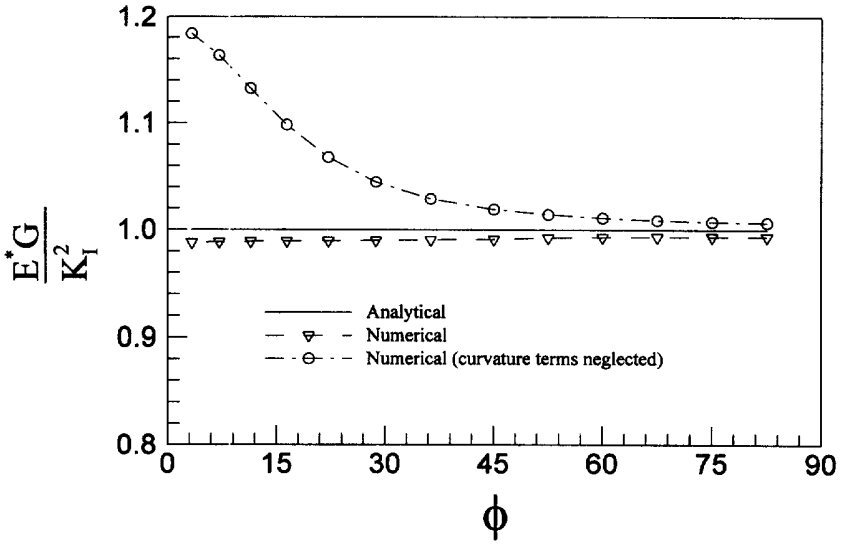

Fig. 12. The energy release rate G (computed from the J-integral) normalized with respect to the stress intensity factor K_I (computed from the interaction energy integral) plotted vs parametric angle ϕ for the case of an elliptical crack embedded in a homogeneous solid.

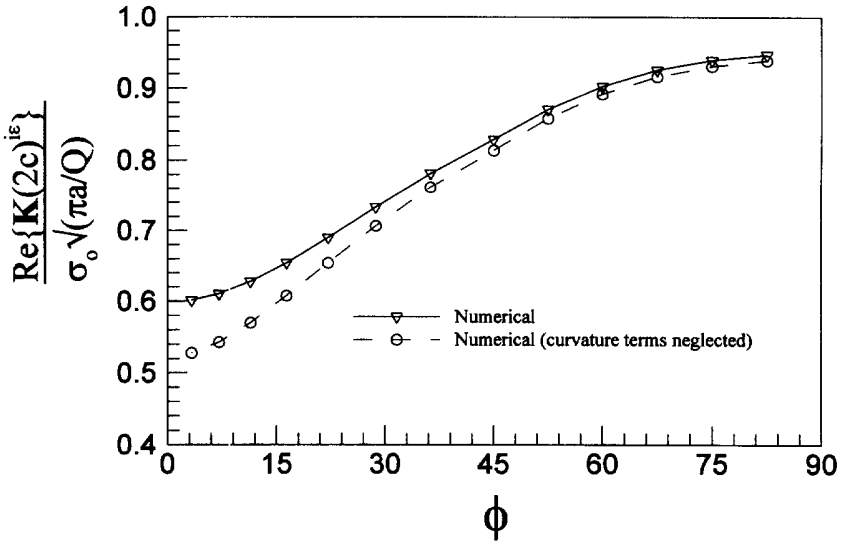

Fig. 13. Normalized stress intensity factor K_I plotted vs parametric angle ϕ for the case of an elliptical bimaterial interface crack between glass and steel.

The phase angle φ reaches a maximum of approximately 91° at the $\phi = 21°$ location, and it approaches 90° ($K_{III} = 0$) at both the $\phi = 0°$ and $\phi = 90°$ locations as one would expect due to the symmetry of the problem.

5. SUMMARY AND CONCLUDING REMARKS

In the present paper, domain representations of interaction energy integrals were derived for evaluating mixed-mode stress intensity factors along curvilinear bimaterial interface cracks. In the derivation, the asymptotic fields for the plane problem of a bimaterial interface crack were imposed along a curved crack front. The general crack-tip interaction integral (a contour integral surrounding a point on the crack front which is evaluated in the limit as the contour is shrunk onto the crack tip) was then expressed in domain form and was evaluated as a post-processing step in the finite element method. As a consequence of imposing the auxiliary fields along a curvilinear crack front, the auxiliary stress fields do

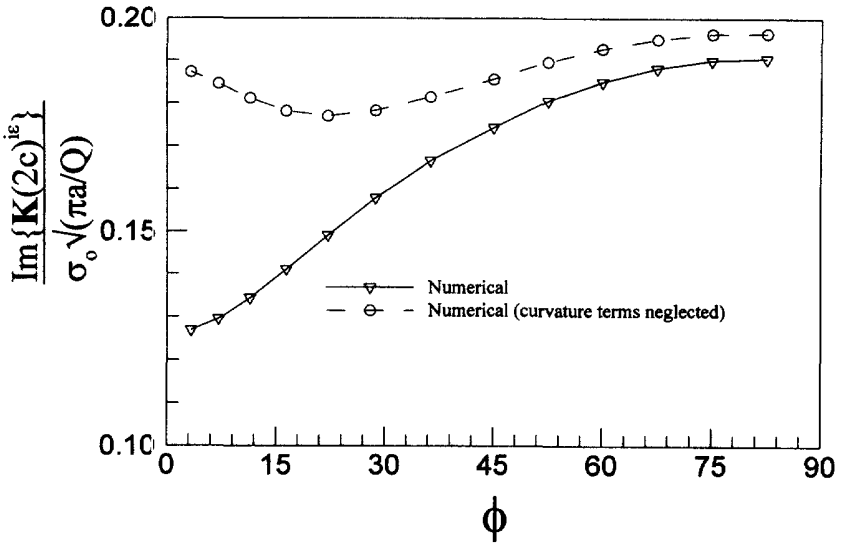

Fig. 14. Normalized stress intensity factor K_{II} plotted vs parametric angle ϕ for the case of an elliptical bimaterial interface crack between glass and steel.

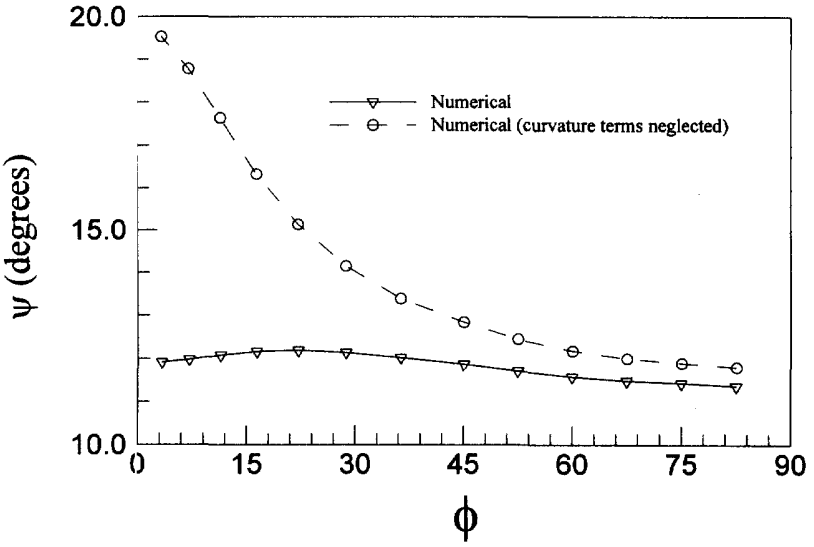

Fig. 15. The phase angle ψ ($L = 2c$) plotted vs parametric angle ϕ for the case of an elliptical bimaterial interface crack between glass and steel.

not satisfy equilibrium, and the auxiliary strain fields are incompatible with the auxiliary displacement fields. Because of the lack of equilibrium and compatibility, along with other local curvature affects, additional terms must be included in the resulting domain integrals. In the numerical results, it was demonstrated that it is crucial to maintain these additional terms, especially when the local crack front curvature is high. In the paper, we presented two numerical examples. As a benchmark, we first considered the problem of a penny-shaped interface crack embedded in a cylinder. The results for the complex stress intensity factor and phase angle were found to be in excellent agreement with the analytical solution. The problem of an elliptical crack embedded between two dissimilar isotropic materials was also considered. It was found that the mismatch in the elastic constants between the two materials caused significant mode II loading near the crack tip, and it was found that the phase angle ψ remained relatively constant along the entire crack front. The mode III stress intensity factor along the crack front was found to be very small compared to the mode I and mode II stress intensity factors. In all cases, the results were found to be in significant error when the additional curvature terms were neglected.

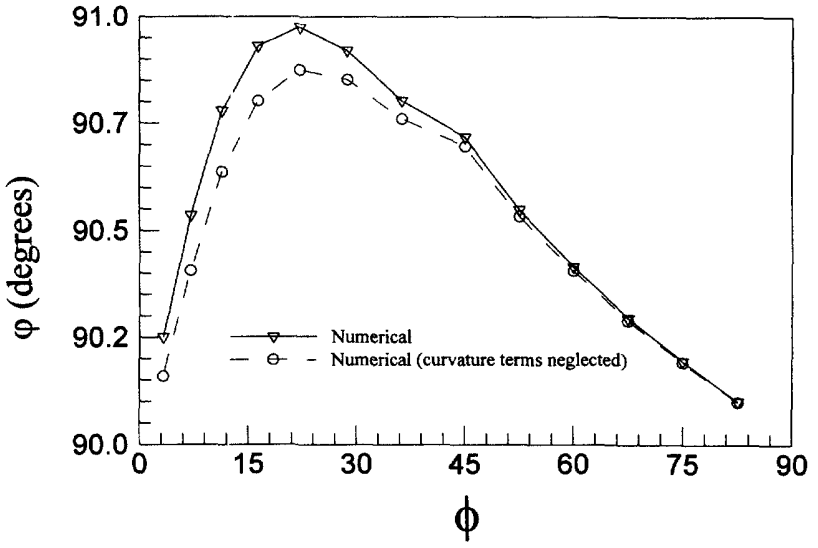

Fig. 16. The phase angle φ plotted vs parametric angle ϕ for the case of an elliptical bimaterial interface crack between glass and steel.

As a final remark, we note that the method presented in this paper may be extended to the case of a curved bimaterial interface crack between dissimilar anisotropic materials. This will involve using the near-tip fields for the plane problem of an interface crack between different anisotropic materials in the interaction energy integrals.

Acknowledgements—The authors are grateful for the support provided by the IBM T. J. Watson Research Center, Yorktown Heights NY. Helpful discussions with Dr Rakesh Nahta are also gratefully acknowledged.

REFERENCES

Eshelby, J. D. (1956) The continuum theory of lattice defects. In *Solid State Physics*, eds F. Seitz and D. Turnbull, Vol. 3, pp. 79–141. Academic Press, New York.

Eshelby, J. D. (1970) Energy relations and the energy momentum tensor in continuum mechanics. In *Inelastic Behavior of Solids*, eds M. F. Kanninen, W. F. Adler, A. R. Rosenfeld and R. T. Jaffee, pp. 77–114. McGraw-Hill, New York.

Hutchinson, J. W. and Suo, Z. (1991) Mixed mode cracking in layered materials. In *Advances in Applied Mechanics*, Eds J. W. Hutchinson and T. Y. Wu, Vol. 29, pp. 63–191. Academic Press, San Diego.

Irwin, G. R. (1962) The crack extension force for a part through crack in a plate. *Journal of Applied Mechanics, Transactions of the American Society of Mechanical Engineers*, **29**(4), 651–654.

Kassir, M. K. and Bregman, A. M. (1972) The stress intensity factor for a penny-shaped crack between two dissimilar materials. *Journal of Applied Mechanics*, **39**, 308–310.

Li, F. Z., Shih, C. F. and Needleman, A. (1985) A comparison of methods for calculating energy release rates. *Engineering Fracture Mechanics*, **21**, 405–421.

Moran, B. and Shih, C. F. (1987a) A general treatment of crack tip contour integrals. *International Journal of Fracture*, **35**, 295–310.

Moran, B. and Shih, C. F. (1987b) Crack tip and associated domain integrals from momentum and energy balance. *Engineering Fracture Mechanics*, **27**(6), 615–642.

Nahta, R. and Moran, B. (1993) Domain integrals for axisymmetric interface crack problems. *International Journal of Solids and Structures*, **30**(15), 2027–2040.

Nakamura, T. and Parks, D. M. (1989) Antisymmetrical 3-D stress field near the crack front of a thin elastic plate. *International Journal of Solids and Structures*, **25**(12), 1411–1426.

Nakamura, T. (1991) Three-dimensional stress fields of elastic interface cracks. *Journal of Applied Mechancis*, **58**, 939–946.

Nikishkov, G. P. and Atluri, S. N. (1987) Calculation of fracture mechanics parameters for an arbitrary three-dimensional crack by the 'equivalent domain integral method'. *International Journal of Numerical Methods in Engineering*, **24**, 1801–1821.

Rice, J. R. (1988) Elastic fracture mechanics concepts for interfacial cracks. *Journal of Applied Mechanics*, **55**, 98–103.

Rice, J. R., Suo, Z. and Wang, J. S. (1990) Mechanics and thermodynamics of brittle interfacial failure in bimaterial systems. In *Metal-Ceramic Interfaces*, eds M. Ruhle, A. G. Evans, M. F. Ashby and J. P. Hirth, pp. 269–294. Pergamon Press, Oxford.

Shih, C. F. (1990) Cracks on bimaterial interfaces: elasticity and plasticity aspects. *Material Science Engineering*, **A143**, 77–90.

Shih, C. F. and Asaro, R. J. (1988) Elastic-plastic analysis of cracks on bimaterial interfaces: part I—small scale yielding. *Journal of Applied Mechanics*, **55**, 299–316.
Shih, C. F., Moran, B. and Nakamura, T. (1986) Energy release rate along a three-dimensional crack front in a thermally stressed body. *International Journal of Fracture*, **30**, 79–102.

APPENDIX A

A brief description of the finite element evaluation of the domain representations for the energy release rate and the interaction energy integrals introduced in Section 2 is outlined below. In order to illustrate the procedure, we consider the situation where the volume V containing a segment of the crack front is discretized with 32 eight-node brick elements as shown in Figs A.1 and A.2. A cross-section of the finite element mesh which is perpendicular to the plane of the crack and passes through a node M which lies on the crack front is illustrated in Fig. A.1. A view of the cross-section which lies in the plane of the crack and passes through M is shown in Fig. A.2. Consistent with a standard isoparametric finite element formulation, we interpolate the test function q_l within an element in V using the trilinear finite element shape functions, i.e.,

$$q_l = \sum_{a=1}^{8} N_a Q_l^a \tag{A-1}$$

where Q_l^a are the discrete nodal values of the test function. In the present analysis we have chosen the nodal values such that

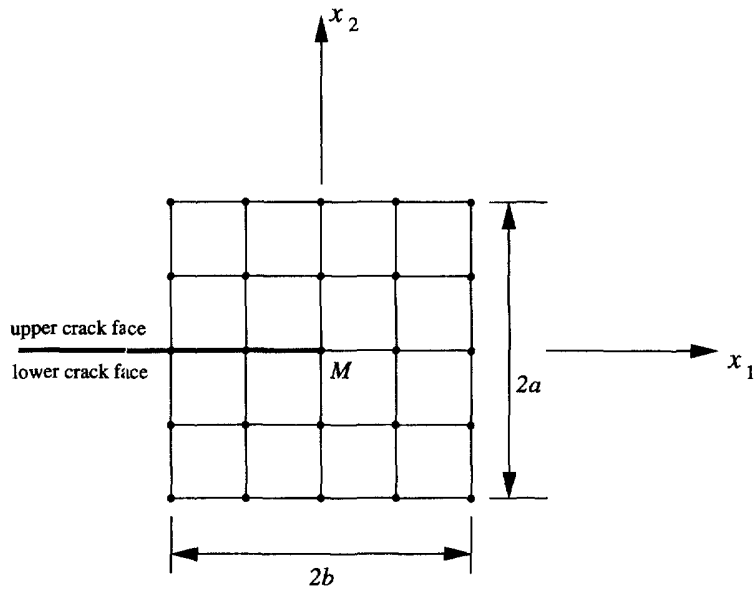

Fig. A.1. Cross-section of finite element mesh which is normal to the plane of the crack and passes through node M.

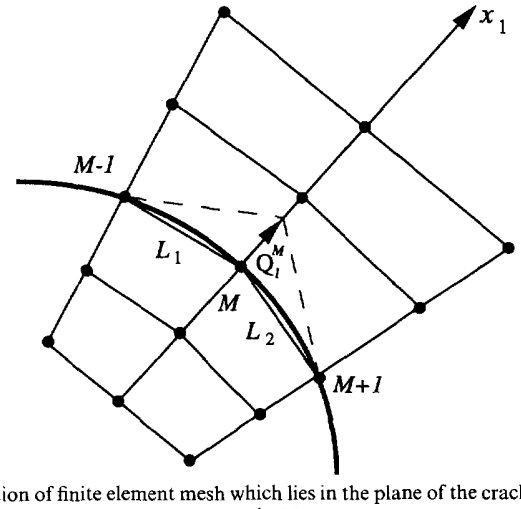

Fig. A.2. Cross-section of finite element mesh which lies in the plane of the crack and passes through node M.

$$Q_l^a = \begin{cases} \xi_l^M & \text{if } x_3^a = 0 \text{ and } |x_2^a| < b \text{ and } |x_1^a| < a \\ 0 & \text{otherwise} \end{cases} \tag{A-2}$$

where the dimensions a and b are defined in Fig. A.1.

The discrete form of the domain integral (18) is then written as

$$\bar{I}^M = -\sum_{e \in V} \left\{ \int_{\Omega_e} (P_{ij} q_{l,j} + P_{ij,j} q_l) \, d\Omega \right\} \tag{A-3}$$

where

$$q_{l,j} = \sum_{a=1}^{8} N_{a,j} Q_l^a. \tag{A-4}$$

In the present analysis, the integration (A-3) was carried out using $2 \times 2 \times 2$ Gauss quadrature. It follows directly from the definition (A-2) that the magnitude of the virtual crack advance $\Delta a(s)$ varies linearly along L_e with $\Delta a(s) = 1$ at node M and $\Delta a(s) = 0$ at nodes M−1 and M+1 as shown in Fig. A.2. Thus, the integral in the denominator of eqn (19) yields

$$\int_{L_e} \Delta a(s) \, ds = \frac{1}{2}(L_1 + L_2) \tag{A-5}$$

and the pointwise value $I(s)$ at node M is given by

$$I^M = \frac{2\bar{I}^M}{L_1 + L_2} \tag{A-6}$$

where L_1 and L_2 are the lengths of the chords defined in Fig. A.2.

A detailed computational procedure for evaluating the pointwise value $I(s)$ at node M is given in Table 2.

Table 2. Computational procedure for evaluating I^M

1. Compute the components of the unit outward normal to the mathematical crack front at node M.
2. Loop over elements $e = 1,2,\ldots$:
   - 2.1 Compute element nodal coordinates in local crack-tip coordinate system with origin at mode M.
   - 2.2 If $e \in V$ go to Step 2.3; else go to next element, Step 2.
   - 2.3 Compute the nodal values Q_l^a of the test function q_l.
   - 2.4 Set up integration points and weights ($2 \times 2 \times 2$ quadrature employed).
   - 2.5 Loop over integration points $l = 1$ to 8.
     - 2.5.1 Evaluate the shape functions N_a and global derivatives $\partial N_a / \partial X_k$ at the integration point.
     - 2.5.2 Evaluate the test function q_l and global derivatives $\partial q_l / \partial X_k$ at the integration point.
     - 2.5.3 Set up new local crack-tip coordinate system as follows:
       - a. Compute the global coordinates of the integration point p.
       - b. Determine the coordinates of point P', the projection of the integration point onto the plane of the crack front.
       - c. Find the point s on the mathematical crack front that is closest to the point P'. The coordinates of point s are obtained by minimizing the distance formula using, e.g., Newton's Method. Point s becomes the origin of the local crack-tip coordinate system.
     - 2.5.4 Determine the coordinates of the integration point p in the local crack-tip coordinate system.
     - 2.5.5 Calculate the radius of curvature ρ_s of the mathematical crack front at point s.
     - 2.5.6 Using eqn (24), calculate the radius of curvature ρ of the coordinate curve ξ_3 (see Fig. 5) at the integration point p. It is also necessary in this step to compute the derivatives $\partial\rho/\partial\xi_1$ and $\partial\rho/\partial\xi_3$ which appear in certain components of the tensor $\overrightarrow{\nabla}\mathbf{u}^{aux}\overleftarrow{\nabla}$ when extracting the mode I and mode II stress intensity factors.
     - 2.5.7 Calculate the local crack-tip angle θ (see Fig. 5).
     - 2.5.8 Compute the distance, r, from point s to the integration point p.
     - 2.5.9 Compute the integrand as follows:
       - a. Compute $\mathrm{tr}[(W\mathbf{1} - \overrightarrow{\nabla}\mathbf{u} \cdot \boldsymbol{\sigma}) \cdot \overrightarrow{\nabla}\mathbf{q}]$ for J-integral.
       - b. Given r, θ, and ρ, compute $\mathrm{tr}(\mathbf{P} \cdot \overrightarrow{\nabla}\mathbf{q}) + (\overrightarrow{\nabla} \cdot \mathbf{P}^T) \cdot \mathbf{q}$ for interaction energy integral. It is convenient to express the components of all of the tensors ($\overrightarrow{\nabla}\mathbf{u}$, $\overrightarrow{\nabla}\mathbf{u}^{aux}$, $\overrightarrow{\nabla}\mathbf{u}^{aux}\overleftarrow{\nabla}$, ε^{aux}, $\varepsilon^{aux}\overleftarrow{\nabla}$, σ, σ^{aux}, $\mathbf{q}$, and $\overrightarrow{\nabla}\mathbf{q}$) in the local crack-tip coordinate system set up in step 2.5.3.
     - 2.5.10 Add the contribution computed in step 2.5.9 to $\bar{I}^M$.
     - 2.5.11 Go to the next integration point, Step 2.5.
   - 2.6 Go to the next element, Step 2.
3. Compute I^M from eqn (A-6).

APPENDIX B

In this appendix we provide the auxiliary displacement fields that appear in the integrand of the interaction energy integrals defined in Section 2. For the extraction of the mode I and mode II stress intensity factors, the components of the auxiliary displacement fields in the local x_1-x_2 plane (see Fig. 2) are written as

$$u_i^{aux} = \frac{1}{4\mu\cosh(\pi\varepsilon)}\sqrt{\frac{r}{2\pi}}f_i(r,\theta,\varepsilon,\mu) \quad i \to 1 \text{ to } 2. \tag{B-1}$$

To extract K_I, the functions f_i to be used in eqn (B-1) are given as

$$\begin{aligned} f_1(r,\theta,\varepsilon,\mu) &= D+2\delta\sin\theta\sin\phi \\ f_2(r,\theta,\varepsilon,\mu) &= -C-2\delta\sin\theta\cos\phi \end{aligned} \tag{B-2}$$

whereas to extract K_{II}, the functions are given by

$$\begin{aligned} f_1(r,\theta,\varepsilon,\mu) &= -C+2\delta\sin\theta\cos\phi \\ f_2(r,\theta,\varepsilon,\mu) &= -D+2\delta\sin\theta\sin\phi. \end{aligned} \tag{B-3}$$

The constants C, D, δ, and ϕ that appear in (B-2) and (B-3) are defined as follows:

$$\begin{aligned} \delta &= e^{-(\pi-\theta)\varepsilon} \\ \phi &= \varepsilon\ln(r)+\frac{\theta}{2} \\ C &= \bar{\beta}\gamma\cos\frac{\theta}{2}-\beta\bar{\gamma}\sin\frac{\theta}{2} \\ D &= \beta\gamma\cos\frac{\theta}{2}-\bar{\beta}\bar{\gamma}\sin\frac{\theta}{2} \\ \beta &= \frac{0.5\cos(\varepsilon\ln r)+\varepsilon\sin(\varepsilon\ln r)}{0.25+\varepsilon^2} \\ \bar{\beta} &= \frac{0.5\cos(\varepsilon\ln r)-\varepsilon\sin(\varepsilon\ln r)}{0.25+\varepsilon^2} \\ \gamma &= \kappa\delta-\frac{1}{\delta} \\ \bar{\gamma} &= \kappa\delta+\frac{1}{\delta} \\ \kappa &= 3-4\nu. \end{aligned} \tag{B-4}$$

We note the auxiliary disp acement components defined by eqn (B-1) through (B-4) above are valid for points that lie in the upper half-plane (material 1) according to the convention depicted in Fig. 2. To obtain the displacement components in the lower half-plane (material 2), we simply replace π with $-\pi$ in the definition of δ given in (B-4).

For the extraction of the mode III stress intensity factor, the component u_3^{aux} is the only nonzero auxiliary displacement component and is given as

$$\begin{aligned} u_3^{aux} &= \frac{2}{\mu_1}\left(\frac{r}{2\pi}\right)^{1/2}\sin\frac{\theta}{2} \quad \text{upper half-plane} \\ u_3^{aux} &= \frac{2}{\mu_2}\left(\frac{r}{2\pi}\right)^{1/2}\sin\frac{\theta}{2} \quad \text{lower half-plane.} \end{aligned} \tag{B-5}$$

The auxiliary strain components are obtained from the auxiliary displacement components as follows:

$$\begin{aligned} \varepsilon_{11}^{aux} &= u_{1,1}^{aux} \\ \varepsilon_{22}^{aux} &= u_{2,2}^{aux} \\ \varepsilon_{12}^{aux} &= \frac{1}{2}(u_{1,2}^{aux}+u_{2,1}^{aux}) \end{aligned}$$

$$\varepsilon_{13}^{aux} = \varepsilon_{23}^{aux} = \varepsilon_{33}^{aux} = 0 \tag{B-6}$$

for extracting the mode I and II stress intensity factors, and

$$\varepsilon_{13}^{aux} = \frac{1}{2}(u_{1,3}^{aux} + u_{3,1}^{aux})$$

$$\varepsilon_{23}^{aux} = \frac{1}{2}(u_{2,3}^{aux} + u_{3,2}^{aux})$$

$$\varepsilon_{11}^{aux} = \varepsilon_{22}^{aux} = \varepsilon_{33}^{aux} = \varepsilon_{12}^{aux} = 0 \tag{B-7}$$

for extracting the mode III stress intensity factor. For each case, the auxiliary stress fields are obtained from the auxiliary strain fields using Hooke's law.